# Comparison of different numerical methods used to handle the open boundary of a regional ocean circulation model of the Bay of Biscay

Sylvain Cailleau, Veronika Fedorenko, Bernard Barnier, Eric Blayo, Laurent Debreu

# Comparison of different numerical methods used to handle the open boundary of a regional ocean circulation model of the Bay of Biscay

S. Cailleau[a,*], V. Fedorenko[b], B. Barnier[a], E. Blayo[b], L. Debreu[b]

[a]CNRS and University of Grenoble, Laboratoire des Ecoulements Geophysiques et Industriels, Mercator-Ocean, 8/10 rue Hermès, Parc Technologique du canal, 31520 Ramonville, St. Agne, France

[b]University of Grenoble and INRIA, Laboratoire Jean Kuntzmann, BP 53X, 38041 Grenoble Cedex, France

Several methods for specifying boundary conditions at the limits of a regional model are compared. The methods investigated are those using clamped and radiation boundary conditions, one-way and two-way nesting in a model for a more extensive area, and "full" coupling based on domain decomposition tech-niques. These methods are compared in the realistic framework of interactions between a 1/15° model of the Bay of Biscay and a 1/3° model of the North Atlantic, over a 3-year simulation (1996–1998). The clamped and radiation boundary conditions systematically lead to energy accumulation and problematic recirculations along the boundary, and can disturb the internal dynamics of the regional domain. The one-way or two-way-nesting and the full-coupling methods result in far more satisfactory behaviour. For long periods of integration, the two-way mode improves both the fine and coarse-grid solutions. The full coupling method provides the most regular solution at the boundary, and also opens interesting new perspectives since it should enable the coupling of models with different physics. However it requires much more computation time.

## 1. Introduction

Multi-scale modelling in physical oceanography aims at studying ocean physical processes and their interactions over extended spatial and time scales (from mesoscale eddies to the general circulation, and from days to decades, for example). The concept is as follows: a large-scale model (global or basin-scale model) provides information for regional models whose resolution is thus improved; the latter models then eventually feed back information to the larger model. A major difficulty in this approach lies in the exchange of information at the boundaries of the regional model. Indeed, the conditions applied at the boundaries of the regional model must provide it with the relevant information from outside, while at the same time exporting the model's outgoing information and without disturbing the internal solution. This latter point becomes crucial when the regional model is also to be used to correct the large-scale model solution.

This study investigates the importance of the method (referred to as the coupling method hereafter, although this term will not be accurate for some methods) used to specify information at the open boundary in the solution of a particular large-scale/regional model system.

* Corresponding author. Tel.: +33 (0) 5 61 39 38 38.
*E-mail address:* sylvain.cailieau@mercator-ocean.fr (S. Cailleau).

Two models based on the same numerical code are considered. A regional model of the Bay of Biscay with a high resolution (1/15° grid), and a large-scale North Atlantic model of coarser resolution (1/3° grid). Both models can be run in stand-alone mode, but the regional model can also be embedded in or coupled with the large-scale model. Thus, it is possible to test and compare the results obtained by the regional model when driven at its open boundaries by the large-scale model using different methods for exchanging information. This study compares three different types of coupling methods; the commonly used methods such as those involving clamped or radiative open boundary conditions (Tréguier et al., 2001; Marchesiello et al., 2001; Barnier et al., 1998), a grid refinement method (or nesting) as used in the studies of Chanut et al. (2008), Penven et al. (2003), Debreu (2000), and a full coupling method developed for this work, referred to as the Schwarz method.

Most methods considered here have been evaluated in idealised studies, but rarely compared. Tréguier et al. (2001) compared the efficiency of the radiative condition with that of the clamped condition in an eddy-resolving model of the Atlantic with two open boundaries. In this situation, both methods were found to be quite similar. The choice of available external data to be applied to the boundaries seems to have been more determinant. Fox and Maskell (1995) analysed the behaviour of one-way and two-way 3-km grid refinements around the Faroe Islands in a 9-km grid

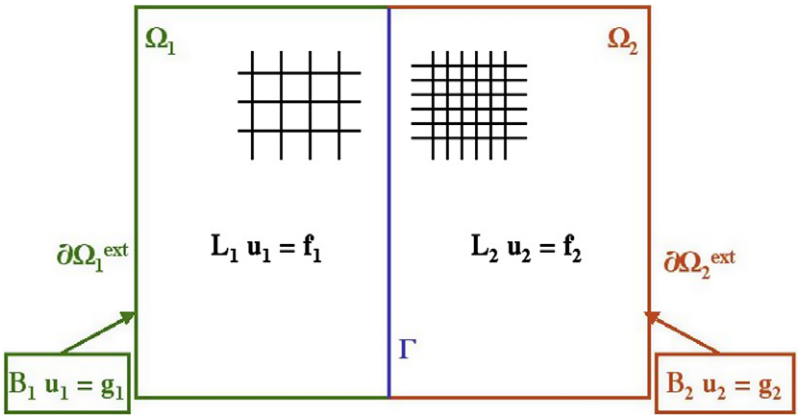


**Fig. 1.** Schematic view of the two numerical models of ocean circulation in the domains $\Omega_1$ and $\Omega_2$. The mathematical notations correspond to those introduced in Section 2.3. The portions of meshes symbolize the different resolutions of the models.

model of the North-East Atlantic. The one-way mode refinement led to permanent noise along the boundary.

In view of the growing importance of multi-scale modelling, especially for ocean forecasting, and of the persistent difficulty posed by the numerical treatment of open boundaries in limited area ocean models, it appears interesting to compare these various methods in a realistic application. This paper presents the results of such a comparison using a model of the Bay of Biscay driven at its open boundary by a model of the North Atlantic.

The paper is organised as follows. The different methods of constraint used to exchange information between the two models are described in Section 2. The models, as well as the simulation strategy, are described in Section 3. Finally, the results comparing the impact of the boundary condition methods on the solution inside the Bay of Biscay are discussed in Section 4.

## 2. Coupling methods

Several coupling methods have been applied and compared in our realistic test case. These methods can be (rather arbitrarily) classified into three categories: *open boundary conditions* (for which the term "coupling" is inaccurate), *1-way* and *2-way nesting*, and *full coupling*.

Before describing these methods further, let us first introduce some notations. We use $\Omega_i$ to denote the geographical domain of model $i$, where the index $i = 1$ corresponds to the large-scale model and $i = 2$ to the regional model. $\Gamma$ is the interface between $\Omega_1$ and $\Omega_2$, i.e. the open boundary of $\Omega_2$ located in the interior of $\Omega_1$. Depending on the coupling method, we consider cases where $\Omega_1$ fully or partially overlaps $\Omega_2$, and cases where it does not (see Fig. 1).

### 2.1. Open boundary conditions

This category of methods corresponds to the case when the regional model is run alone. It is forced at its open boundaries using external data obtained, for example, from climatological databases or from a previous simulation of the large-scale model. The quality of the results therefore depends mainly on two aspects. One is the quality of the external data (typically their time and space resolution and their consistency with the physics of the regional model). The other aspect is the open boundary condition (OBC), i.e. the mathematical condition that is applied to the model variables at the open boundaries, and which involves the external data. The problem of designing OBCs in the context of ocean and atmosphere models has been addressed by numerous papers for more than 30 years. For a review of these studies, one can refer for instance to the introductory parts of the papers by Palma and Matano (1998), Marchesiello et al. (2001), Tréguier et al. (2001), or the review papers by Givoli (1991), Tsynkhov (1998) or Holstad and Lie (1999).

We choose here to test two OBCs that are widely used in ocean modelling. The first is the so-called *clamped* (or Dirichlet) BC. This can be written as $\phi = \phi^{ext}$ on $\Gamma$, where the superscript *ext* denotes external data, for each model variable $\phi$.

The second OBC is a *radiation* BC. Since the work of Orlanski (1976), numerous variants of this type of method have been proposed. We choose here to use the formulation proposed by Marchesiello et al. (2001):

$$\frac{\partial \phi}{\partial t} + c_x \frac{\partial \phi}{\partial x} + c_y \frac{\partial \phi}{\partial y} = -\frac{\phi - \phi^{ext}}{\tau} \qquad \text{on } \Gamma \tag{1}$$

for any model variable $\phi$. It is thus composed of a transport condition (left hand side), combined with a relaxation term to external data (right hand side). At every gridpoint along the open boundary, radiation conditions estimate adaptively at every time step the values of $c_x$ and $c_y$. Depending on the sign of $c_x$ and $c_y$, $\phi$ is considered as locally incoming or outgoing. If considered as incoming, the OBC is modified to:

$$\frac{\partial \phi}{\partial t} = -\frac{\phi - \phi^{ext}}{\tau_{in}} \qquad \text{on } \Gamma \tag{2}$$

which relaxes $\phi$ towards the external value $\phi^{ext}$ with a short timescale $\tau_{in}$. If $\phi$ is considered as outgoing, then the full Eq. (1) is used, with a longer relaxation timescale $\tau_{out} \gg \tau_{in}$, i.e. with a much weaker relaxation towards $\phi^{ext}$ (see Marchesiello et al., 2001 for a detailed description of the method).

Note that, as mentioned earlier, we choose to use these two OBCs in our test bed because of their wide application in previous and current simulations. Radiation conditions have been applied in numerous studies, often in conjunction with a sponge layer and some mass conservation constraint (e.g. Perkins et al., 1997; Barnier et al., 1998; Marchesiello et al., 2001; Tréguier et al., 2001; Penven et al., 2006). They yielded reasonable results, in the sense that they allow for stable multi-year integration of the model, with a rather smooth behaviour of the solution in the vicinity of the boundary and a correct representation of the main statistical features of the interior ocean circulation. In this study, the implementation of the radiation OBC is that described by Tréguier et al. (2001) for the CLIPPER Atlantic model, since the same numerical model as CLIPPER is used (see Section 3.1).

### 2.2. One-way and two-way nesting

In these methods, both the large-scale model and the regional model are run. The solution to the large-scale model is then used as external data in the OBCs of the regional model. This is called *one-way interaction*, which for the regional model is very close to the OBC configuration described earlier. The main difference lies in the quality and the time and space resolution of these external data, which are made available at the time and space resolution of the large-scale model. Note that in this approach the large-scale model does not "see" (i.e. is not affected by) the regional model. Both models can even be run separately, with the results of the large-scale model the regional being used "off-line" by the regional model. In our implementation of this one-way method, we chose to use clamped conditions as OBCs for the regional model, since radiation conditions and clamped conditions lead to very similar results in the simulations of the regional model alone (see Section 4).

In the *two-way approach*, on the other hand, both models must be run simultaneously, with on-line interaction, since a retroaction phase is added from the regional model into the large-scale model. This retroaction is usually operated at every time step of the large-scale model. It consists in updating its solution in the area corresponding to the regional model (i.e. $\Omega_1 \cap \Omega_2$), using the solution of the latter. This is usually done by simply copying the regional model solution onto the large-scale model solution or by applying a local average of the former to the latter. Moreover, in order to avoid mass unbalance, the velocity field of the regional model along $\Gamma$ is locally adjusted at each large-scale model time step, thus ensuring equal mass fluxes between both models.

Note that, depending on the applications, the regional model grid may (or may not) be an exact refinement of the large-scale model grid. If it is an exact refinement, the grid interactions (interpolation and restriction) are made easier, since mapping between the two grids is very simple and regular (see, for example, Debreu et al., 2008 for details). If this is not the case, mapping is more complex, as indeed are the interpolation and restriction operators. However, for a given ratio between the mesh sizes of both models, the question of whether mapping is very regular or not does not significantly affect the solutions as soon as the interpolation operator is of sufficiently high order. Indeed we tested both cases in the realistic configuration described in the present paper, and observed no significant changes in the solution.

### 2.3. "Full coupling" methods

In the above one-way and two-way nesting algorithms, which are the methods commonly used in actual oceanographic applications, the connection between the two model solutions through $\Gamma$ cannot be very regular. We cannot for instance obtain continuity in both the model variables and their fluxes. The one-way and two-way (without flux correction) methods only ensure continuity of the model variables, while the two-way method with flux correction ensures continuity of the fluxes, but no longer continuity of the variables. To address this problem so as to obtain a solution closer to the exact mathematical solution of the coupled problem, more sophisticated coupling methods must be considered. A possible approach is to use the framework of domain decomposition. Domain decomposition methods have been intensively studied and developed since the end of the 1980s thanks to the advent of parallel computers. Among these methods, the global in-time Schwarz method is particularly well suited to the present coupling problem. The principle of this iterative method is summarised below.

Let us decompose the total duration of the simulation into successive time windows of fixed length. We note symbolically $L_i u_i = f_i$ the equations of model $i$ ($i = 1, 2$), and we assume that we are looking for a continuous and differentiable connection between $u_1$ and

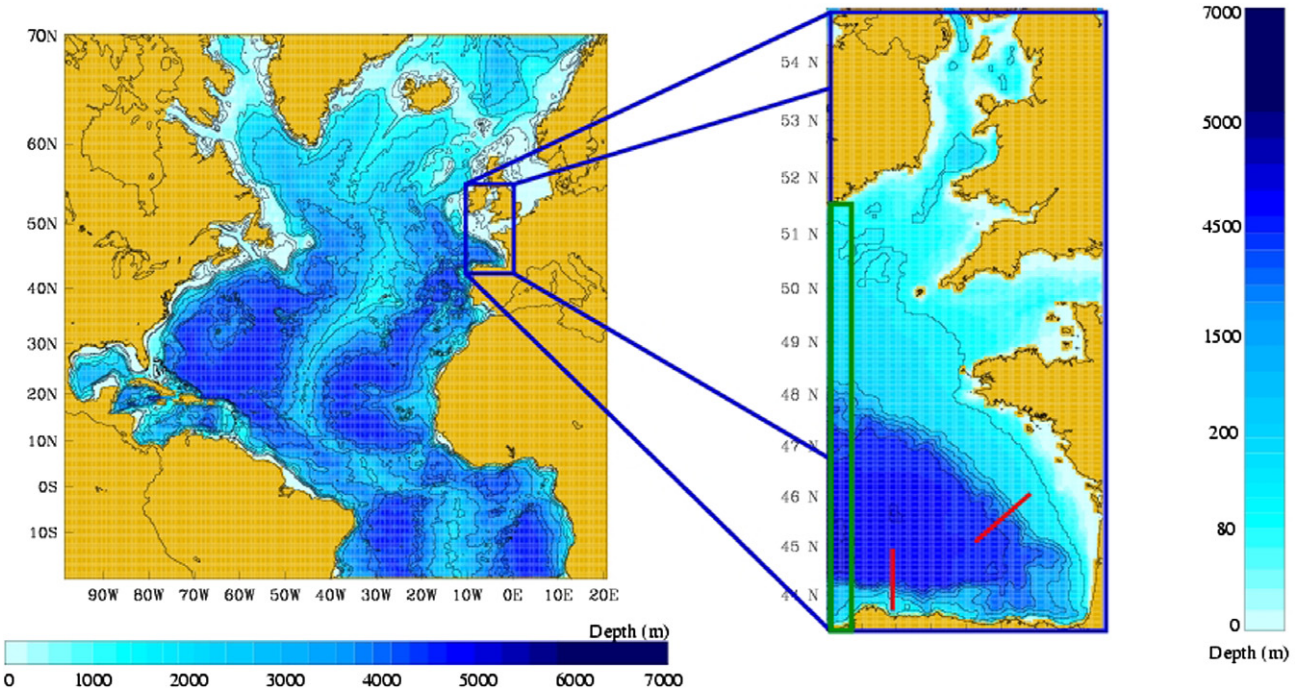


**Fig. 2.** Domain and bathymetry of the NATL3 large-scale model (1/3° resolution) and of the BABY15 regional model (1/15° resolution). The red lines correspond to the sections used to calculate the transport in Fig. 13. The area within the green box is the transition layer where the viscosity/diffusivity coefficients gradually move from the values of the large model to those of the regional model. It is also the region where the bottom topography is smoothed to remove a discontinuity at the boundary. (For interpretation of the references to color in this figure legend, the reader is referred to the web version of this article.)

$u_2$ through $\Gamma$. For each time window $[t_k,t_{k+1}]$, the problem is then to find $u_1$ and $u_2$ that satisfy

$$\begin{cases} L_1 u_1 = f_1 \quad \text{in } \Omega_1 \times [t_k, t_{k+1}] \quad \text{and} \quad L_2 u_2 = f_2 \quad \text{in } \Omega_2 \times [t_k, t_{k+1}] \\ \quad \text{with } u_1 = u_2 \quad \text{and} \quad \frac{\partial u_1}{\partial n} = \frac{\partial u_2}{\partial n} \quad \text{on } \Gamma \times [t_k, t_{k+1}] \end{cases} \tag{3}$$

where $n$ denotes the normal direction to $\Gamma$. To solve (3), the Schwarz algorithm consists in iterating:

$$\begin{cases} L_1 u_1^{n+1} = f_1 & \text{in} \Omega_1 \times [t_k, t_{k+1}] \\ B_1 u_1^{n+1} = B_1 u_2^n & \text{on} \Gamma \times [t_k, t_{k+1}] \end{cases} \\ \text{and} \begin{cases} L_2 u_2^{n+1} = f_2 & \text{in} \Omega_2 \times [t_k, t_{k+1}] \\ B_2 u_2^{n+1} = B_2 u_1^n & \text{on} \Gamma \times [t_k, t_{k+1}] \end{cases} \tag{4}$$

until the value of $u_1 - u_2$ (in a given norm) along $\Gamma$ becomes small enough. The superscripts denote the number of iterations, and $B_1$ and $B_2$ are interface operators to be chosen. Note that, at each iteration, the two models can be run in parallel over the whole time window $[t_k, t_{k+1}]$. If no parallel computer is available, the interface condition for $u_2$ can be replaced for example by $B_2 u_2^{n+1} = B_2 u_1^{n+1}$, which prevents parallelism but increases the convergence rate of the algorithm.

This rate largely depends on the choice of $B_1$ and $B_2$. The simplest choice consists in choosing $B_1 = B_2 = Id$ (Dirichlet–Dirichlet conditions), which makes the algorithm converge towards the true solution $(u_1, u_2)$ provided that $\Omega_1$ and $\Omega_2$ partially overlap. Much more sophisticated operators can also be considered in order to improve the convergence rate, an important issue for oceanic applications given the computational burden of the models used. However, our aim in the present study is to simply compare the solution given by this "full coupling" approach with the solutions given by more common methods. This is why we did not try to optimize the computation in the present application, and simply used Dirichlet–Dirichlet conditions (see Martin, 2003, 2005 for such optimized approaches applied to 2-D tracer equations and to the shallow-water system).

To the best of our knowledge, this is the first time that such a domain decomposition approach has been used in a fairly realistic ocean modelling context. One of our aims is thus to determine whether improving the local quality of the solution through the interface $\Gamma$ has a substantial impact on the global solution. Moreover, it is important to note that such an approach is quite general, and can be applied to a wide variety of coupling problems.

## 3. Modelling framework and simulation strategy

The framework designed to compare the various numerical methods comprises a large-scale model of the North Atlantic at a resolution of 1/3° (referred to as NATL3) which provides the different types of boundary conditions for a fine-resolution (1/15°) regional model of the BAy of BiscaY (referred to as BABY15). The set-up of each model is briefly described in Section 3.1, and model domains are shown in Fig. 2. Our comparison analysis of the various coupling methods will focus on the major boundary connecting these domains, i.e. the western boundary of the BABY15 domain at 9.2°W.

Both models are an implementation of the primitive equation OPA8.1 numerical code (Madec et al., 1998), a $z$-coordinate, second-order finite difference model of the ocean general circulation with a rigid lid. In the simulation presented here, lateral mixing (momentum and tracers) is modelled by a biharmonic operator, and vertical mixing (momentum and tracers) is calculated using the second order turbulent eddy kinetic energy closure model (Madec et al., 1998).

**Table 1**
Set of 3-year experiments (1996–1998).

| Simulations | Description |
|---|---|
| *NATL3 alone* | 1/3° Large-scale model of the North Atlantic integrated alone |
| *BABY15 clamped* | 1/15° Regional model of the Bay of Biscay integrated alone with clamped western open boundary |
| *1W nesting* | NATL3 model refined on the BABY15 domain in a one-way mode |
| *2W nesting* | NATL3 model refined on the BABY15 domain in a two-way mode |
| *Full coupling* | NATL3 and BABY5 models fully coupled with the Schwarz iterative method |

### 3.1. North Atlantic and regional models

#### 3.1.1. NATL3 large-scale model

The NATL3 model configuration, the bathymetry of which (deduced from Smith and Sandwell, 1997) is shown in Fig. 2, was developed within the CLIPPER Project (Treguier et al., 1999)[1]. It covers the North Atlantic from 98.5°W to 15°E in longitude and from 17°S to 70°N in latitude. The horizontal grid is a Mercator isotropic grid of 1/3° resolution at the equator, and 43 levels are used in the vertical. Many of the details in the configuration and numerical parameters are identical to those described in Tréguier et al. (2001), (see, in particular, their Table 1), for the 1/3° full Atlantic model configuration (from Iceland to Antarctica) from which NATL3 was in fact extracted. In NATL3, zonal northern (70°N) and southern (17°S) boundaries and the strait of Gibraltar are closed. Buffer zones are introduced next to these closed boundaries with the same design as in the DYNAMO experiment (Willebrand et al., 2001); model temperature and salinity fields are relaxed to the climatology of Reynaud et al. (1998) with relaxation time decreasing from 3 days to 100 days as one moves away from the boundaries. The time step of NATL3 is 2400 s. Hyper viscosity/diffusivity are used with a bi-harmonic operator. Coefficients are adjusted to the grid size.

#### 3.1.2. BABY15 fine-grid regional model

The BABY15 regional model configuration was specifically set up for this study. It covers the Gulf of Biscay and the Celtic Shelf up to the Irish Sea (Fig. 2), extending from 9°W to 1°W in longitude and from 43°N to 55°N in latitude. The horizontal grid is a Mercator isotropic grid of 1/15° resolution, and 43 levels are used in the vertical. The bathymetry is deduced from the ETOPO2 data set (http://www.ngdc.noaa.gov). This data set appeared to be less noisy than the topography of Smith and Sandwell (1997) used in NATL3 on the continental shelf. The time step is 480 s. The western boundary (at 9°W) between Galicia and Ireland is open. The northern boundary (between Ireland and Scotland) and the eastern boundary (English Channel) which are 1 and 2 grid point wide, respectively, are closed when the model is run alone, mainly because the algorithm of the radiation condition (Eq. 1) was not adapted to small openings. These two boundaries are open when the model is nested in or coupled with NATL3. The impact of these differences on the model solution are negligible because the model does not include tides, which are the main driver of ocean currents there. Consequently, flows and transports through these boundaries are very weak in the NATL3 model (also because they are shallow passages). In addition, the systematic use of a transition layer adjacent to the boundaries (see Section 3.2.1) where hyper viscosity and diffusivity are increased by a factor of 5 produces a through flow near zero in

[1] The CLIPPER Project (http://www.ifremer.fr/lpo/clipper/ developed a hierarchy of circulation models of the whole Atlantic and of the North Atlantic at resolutions of 1°, 1/3° and 1/6°. All configurations have been validated in numerous publications. They were used to simulate the ocean variability for the WOCE period (1980–2000). The NATL3 configuration was also used by the Mercator-Ocean Centre to perform ocean analyses and forecasts.

all experiments. The opening and closing of these boundaries is found to have no detectable impact on the flow in the Bay of Biscay and the Celtic Shelf, where most model diagnostics are made.

### 3.2. Simulation strategy

Both models are initialised with the temperature and salinity fields of the January mean of 1996, obtained from a previous simulation carried out with the 1/6° resolution ATL6 Atlantic model configuration over the period 1979–2001. This latter model configuration was also set up for the CLIPPER project and is similar to all CLIPPER configurations except for its higher 1/6° resolution. The ATL6 simulation from which our initial conditions are extracted was driven by daily air-sea fluxes from ECMWF re-analysis (ERA15, from 1979 to 1993,) and analyses (from 1994 to 2001). ATL6 has been used in a number of studies to investigate the interannual variability of eddy kinetic energy and heat transport in the North Atlantic (Hall et al., 2004; Lumpkin et al., submitted for publication; Penduff et al., 2004, 2005; Treguier et al., 2006).

All simulations presented in this study start on January 1st, 1996 and last 3 years, from 1996 to 1998. ECMWF daily analyses are used to drive the models (as in the ATL6 simulation) and as in all CLIPPER simulations, fluxes are applied according to the flux correction parameterisation described in Barnier (1998). We checked this initialisation process, performed using the solution of a higher resolution model, to ensure that it ran smoothly and converged rapidly (large-scale features are in place within 3 months).

The set of 3-year experiments designed to compare the various methods used to constrain the BABY15 regional model with the solution of the NATL3 large-scale model is summarized below (see also Table 1).

#### 3.2.1. Large-scale model alone: simulation "*NATL3-alone*"

The large model NATL3 is integrated alone from January 1996 to December 1998. During the 3-year integration of the model, 3-day averages of model variables are stored every 3 days. This simulation provides the reference solution for a 1/3° resolution. It also provides the data (at 3-day intervals) to drive the open boundaries of the BABY15 model over the period 1996–1998.

Before describing the various experiments that were carried out, mention should be made of an important characteristic common to them all: the *transition layer*. Because the change in resolution between the large and the regional domains can be substantial (here a factor of 5), both models will have different values for viscosity and diffusivity coefficients. To avoid a large discontinuity in dissipation which might be a source of numerical instability, we defined a transition layer inside the regional model, adjacent to the open boundary, where the hyper-viscosity/diffusivity coefficients progressively increase from their small interior value (here $2 \times 10^9\,m^4\,s^{-1}$) to the larger value suited for the coarse resolution (here $2.5 \times 10^{11}\,m^4\,s^{-1}$). Our transition layer is as it were similar to a *sponge layer* in which the increase in hyper-viscosity/diffusivity is guided by the ratio between the coarse and the fine grids, and not by the need of damping the dynamics.

The width of the adjacent layer is 15 grid points (here equivalent to 3 grid points of the large model), an ad hoc choice guided by the need to have a progressive increase of hyper-viscosity/diffusivity in the fine grid model, and to have a minimum number of grid points in the coarse model, but enough to calculate a diffusivity in the layer. The bottom topography is also adjusted over this layer. The fine 1/15° topography is progressively smoothed to the 1/3° topography of the large model to avoid sharp discontinuities.

#### 3.2.2. Open boundary conditions: "*BABY15-clamped*" simulation

The BABY15 regional model is integrated alone from 1996 to 1998. At the western open boundary at 9°W, the clamped boundary condition of Section 2.1 is used. Model variables are thus specified at every time step to values linearly interpolated from the 3-day outputs of *NATL3-alone*. Boundaries are closed in the English Channel and the Irish Sea, and buffer zones are used where model temperature and salinity fields are relaxed towards climatological values. We made this choice of closed boundaries because *NATL3-alone* produces very weak flows in the English Channel and the Irish Sea Strait. We also ran an experiment with a radiation condition at 9°W (in line with the method described in Section 2.1, with $\tau_{in} = 1$ day and $\tau_{out} = 1500$ days), and obtained results very similar to those of the clamped BC (not shown) in terms of the statistical behaviour of the interior circulation (mean and eddy characteristics of the flow). A very similar result was found by Tréguier et al. (2001) in a different application of the same numerical code. These authors compared the impact of Fixed OBC versus Radiation OBC in the CLIPPER Atlantic model. Their investigation is based on 3 year-long twin experiments which only differ by the OBCs used, and points out that using Fixed OBC instead of Radiation OBC does not yield any significant difference on the inner model solution (see their section 7). Although we cannot assess any general character to this behaviour (it might be peculiar to the OPA8 numerical code), it justifies that we treat identically Clamped and Radiation OBCs. Therefore the *BABY15-clamped* experiment is the only stand-alone run with BABY15 used in this study. Note that the behaviour of the clamped boundary condition is completely controlled by the enhanced dissipation in the transition layer.

#### 3.2.3. One-way nesting: "*1W-nesting*" simulation

The NATL3 model is refined on the BABY15 region with the 1/15° resolution, in line with the method described in Section 2. This was done using the AGRIF tool (Adaptive Grid Refinement In Fortran, Debreu, 2000; Debreu et al., 2004, 2008; Penven et al., 2006; Chanut et al., 2008), which is a software package allowing an easy introduction of multiresolution capabilities into any structured grid model written in Fortran. The refinement was implemented in such a way that the refined domain and numerical parameters are identical to those of the BABY15 model (in particular bathymetry and forcing in the refined region are exactly the same as in the BABY15 model). Because of the way AGRIF operates, NATL3 and BABY15 appear as two different models (i.e. the NATL3 still calculates a solution on its original grid) and different levels of interaction are possible. In the *1W-nesting* simulation, the NATL3/BABY15 system is integrated for 3 years (1996–1998) in one-way mode, i.e. without any feedback from the fine-grid BABY15 model to the coarse-grid NATL3 model. Thus, the coarse-grid solution is the same as the solution of *NATL3-alone* over the whole NATL3 domain, including the area where the grid is refined. In the refined BABY15 region, we obtain a 1/15° solution which differs from that of *BABY15-clamped* mainly because boundary values provided by the NATL3 model have been updated at every time step (as opposed to interpolated at the time step from 3-day outputs).

#### 3.2.4. Two-way nesting: "*2W-nesting*" simulation

The NATL3/BABY15 system described in the *1W-nesting* simulation is integrated over the 1996–1998 3-year period in a two-way mode. In this mode, the solution of the coarse-resolution NATL3 model in the refined area is obtained by a spatial average on the 1/3° grid of the solution calculated on the fine 1/15° grid of BABY15. The solution of the coarse-grid NATL3 model is consequently influenced at every time step by the 1/15° solution calculated on the fine-grid BABY15 model, and in the refined area is simply a spatially smoothed version of the BABY15 solution. A comparable two-way application of AGRIF is described in Chanut

et al. (2008) where the same NATL3 model is refined to 1/15° in the Labrador Sea to investigate the role of mesoscale eddies on the cycle of convection and restratification.

*3.2.5. Schwarz algorithm: "full-coupling" simulation*

In this simulation, the large model NATL3 and the regional model BABY15 are "fully" coupled, using the Schwarz iterative method described in Section 2.3. In this application, unlike in the earlier nesting cases, there is almost no overlap between the two models (only half a mesh cell), which only interact along their interface $\Gamma$. This means that the grid points of the NATL3 model which overlap the area of the BABY15 model are masked, making "a hole" in the large-scale model. In order to deal with the difference in grid resolutions, interpolation and restriction operators are of course added to exchange information through the interface between the two models.

The number of iterations of the Schwarz algorithm for a given time window (typically 1 day here) is determined by a convergence criterion based on the solutions of the large and regional models along the interface: $\epsilon_1^n = \|u_1^{n+1} - u_1^n\|$ and $\epsilon_2^n = \|u_2^{n+1} - u_2^n\|$. The algorithm is stopped when the solution does not significantly change between two successive iterations, i.e. when $\max(\epsilon_1^n, \epsilon_2^n) < \epsilon$, where $\epsilon$ is a fixed small value. In this study, five iterations were typically sufficient for convergence.

*3.2.6. Computation costs*

The numerical efficiency is often an important issue when dealing with realistic model configurations. That is why it is important to make clear the relative computation burden of the different coupling methods which are considered here. The open boundary problem only requires running the regional model. One-way and two-way nesting require running both the regional and large models (the additional cost corresponding to the interactions between the two models being negligible). Full coupling requires running both models several times (once for each iteration of the Schwarz algorithm). In the present application, the costs of both models are comparable, and the number of iterations for the Schwarz algorithm is typically equal to 5. Therefore the relative costs of the four coupling methods compared to the model alone are roughly 1, 2, 2 and 10.

## 4. Results

In order to evaluate the different boundary conditions, we study their impact on the behaviour of the solution along the boundary and inside the regional domain. An efficient boundary condition should respect several criteria, such as the continuity of instantaneous fields and of integral quantities through the boundary, or the absence of reflection inside the regional model. Such criteria are analysed in this section.

### 4.1. Description of the NATL3-alone and 2W-nesting solutions

In this section, we briefly describe the large model solution *NATL3-alone* in the North East Atlantic region and in the Bay of Biscay, because it constitutes the large-scale forcing of every other simulation presented in this study. Then we compare it to the *2W-nesting* solution, the latter being used as a reference in the following section.

The circulation simulated by *NATL3-alone* reproduces the major circulation features of the area fairly well. Away from the continental slope, the circulation in the North East Atlantic (Fig. 3a) is characterised by a broad and weak zonal eastward flow, which forms the eastern limit of the subtropical gyre. This flow is geostrophic and associated with zonal isopycnals (Fig. 3b). As it reaches the eastern boundary, this broad flow generates a rather energetic current flowing north along the shelf break: this is the slope current of the Bay of Biscay with isopycnals shifting northward at the shelf break (Huthnance, 1984). The seasonal cycle is well simulated in *NATL3-alone*, since the slope current strengthens in autumn when the offshore meridional gradient of isopycnals becomes stronger at the latitude of the Bay (Fig. 3b). The slope current contributes to the Navidad phenomenon described by Pingree and Le Cann

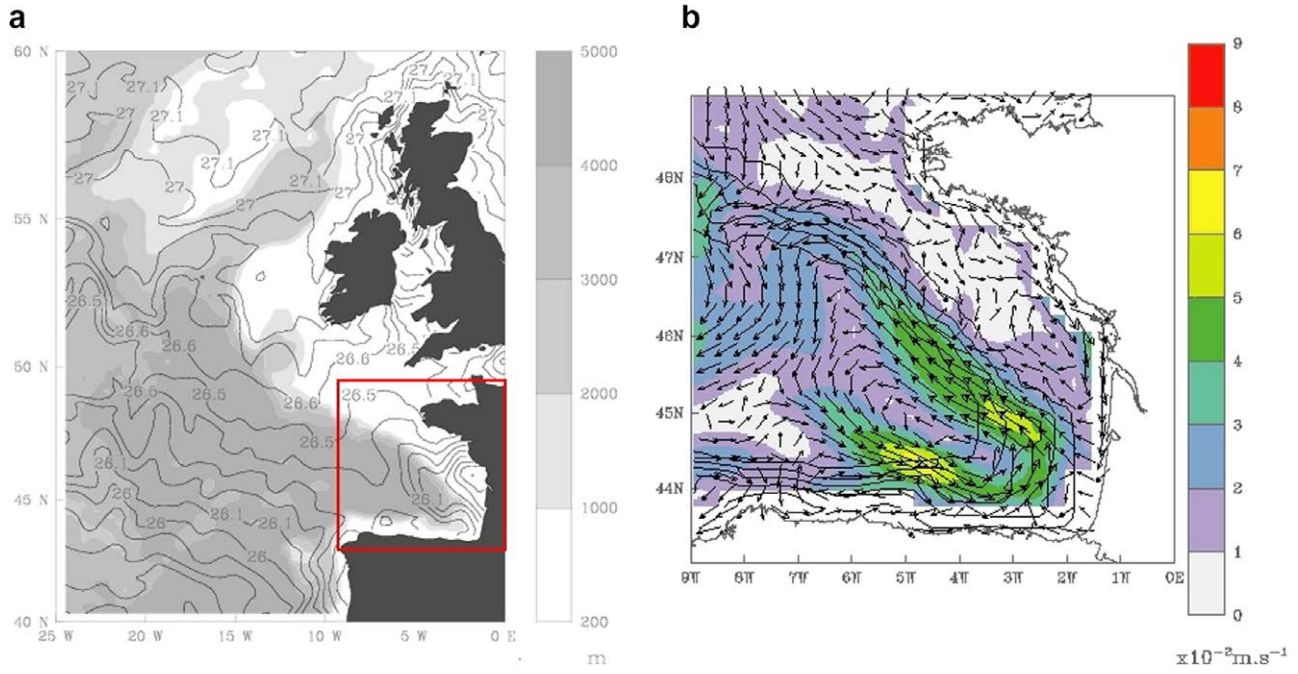


**Fig. 3.** November 1998 mean circulation in the eastern part of the North Atlantic in the *NATL3-alone* simulation: (a) surface potential density field ($\sigma_0$ in kg/m$^{-3}$), the grey colour scale indicating the ocean depth in metres, and (b) velocity field in the zoom indicated by the red box in the figure on the left (our scale indicating current speed in m/s). (For interpretation of the references to color in this figure legend, the reader is referred to the web version of this article.)

(1992): this advection of warm surface water along the shelf break in winter is well represented in *NATL3-alone* (Fig. 4). Thus, the NATL3 model is capable of providing fairly reasonable boundary conditions to the regional high-resolution model over the 3-year period.

The *2W-nesting* solution is qualitatively comparable to that of *NATL3-alone*, but is significantly more energetic. Due to grid refinement, currents and fronts are thinner and stronger, and an important eddy field is observed which was not seen in *NATL3-alone*. In particular, Swoddies (Slope water Oceanic Eddies) very comparable to those observed by Pingree and Le Cann (1992) are generated in *2W-nesting*. The presence of this intense eddy field is quite visible in the temperature field of Fig. 5. Temperature gradients associated with the Navidad are also much better represented in *2W-nesting* (when compared with satellite imagery) than in the coarse solution *NATL3-alone*, due to a better resolution of the slope current along the shelf break. We do not present here a detailed evaluation of the *2W-nesting* solution, since our focus is on the effect of the numerical treatment of the boundary conditions. We rely on the analysis presented in Cailleau's (2004) Ph.D. thesis which demonstrates that *2W-nesting* reproduces most large-scale and mesoscale circulation features of the area, as well as their seasonal variability, in a fairly realistic manner. *2W-nesting* is therefore chosen as a reference for the rest of our study. Note that the suitable behaviour of the AGRIF 2W-nesting procedure has been demonstrated in another application with NATL3 and a grid refinement (to 4 km) in the Labrador Sea (Chanut et al., 2008). In the following subsections, we compare the solutions given by the various methods of coupling in the vicinity of the open boundary and in the interior of the small model domain.

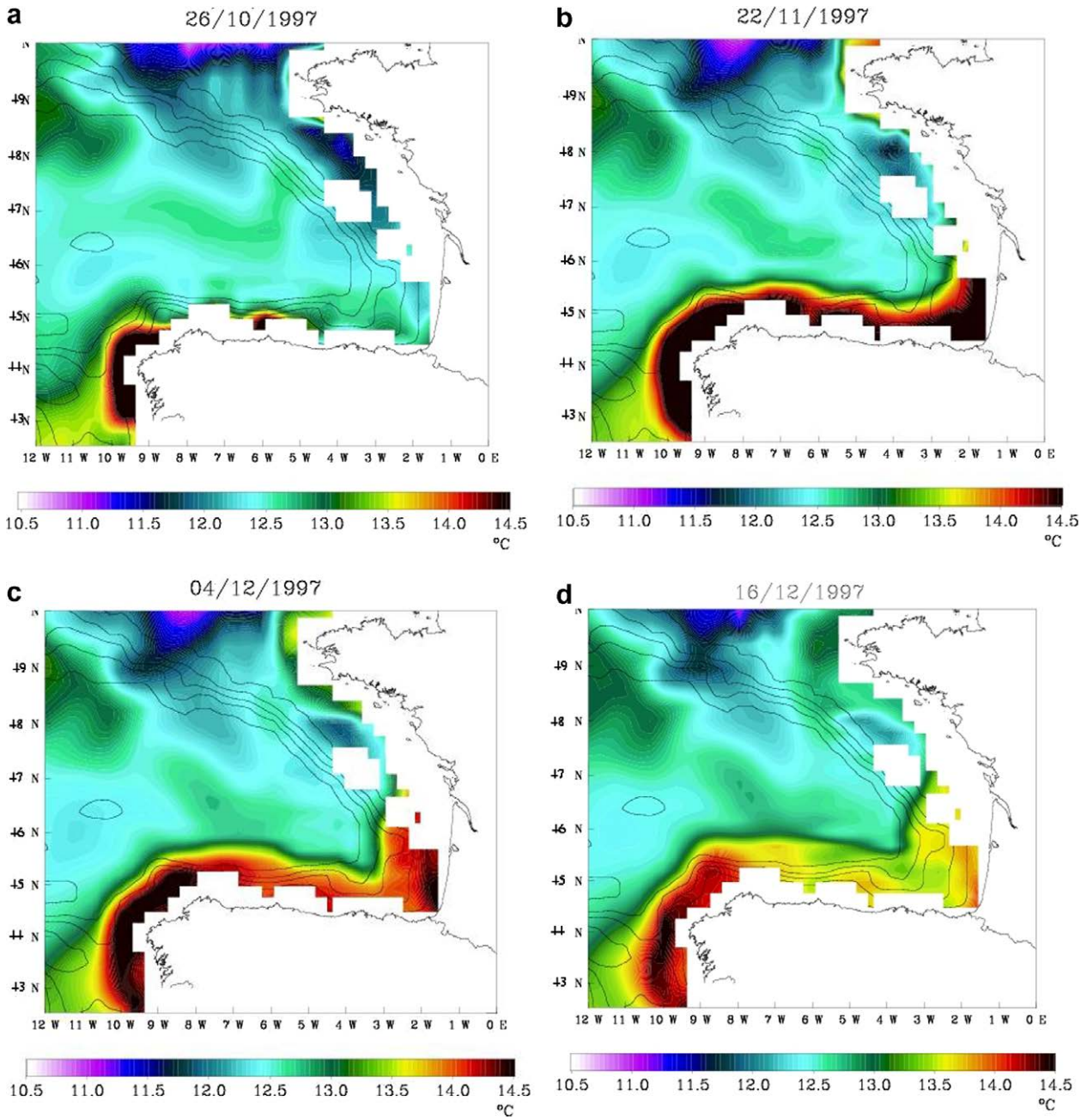


**Fig. 4.** *NATL3-alone* simulation. Four consecutive temperature snapshots at 75 m depth in late 1997 separated by a 15-day interval.

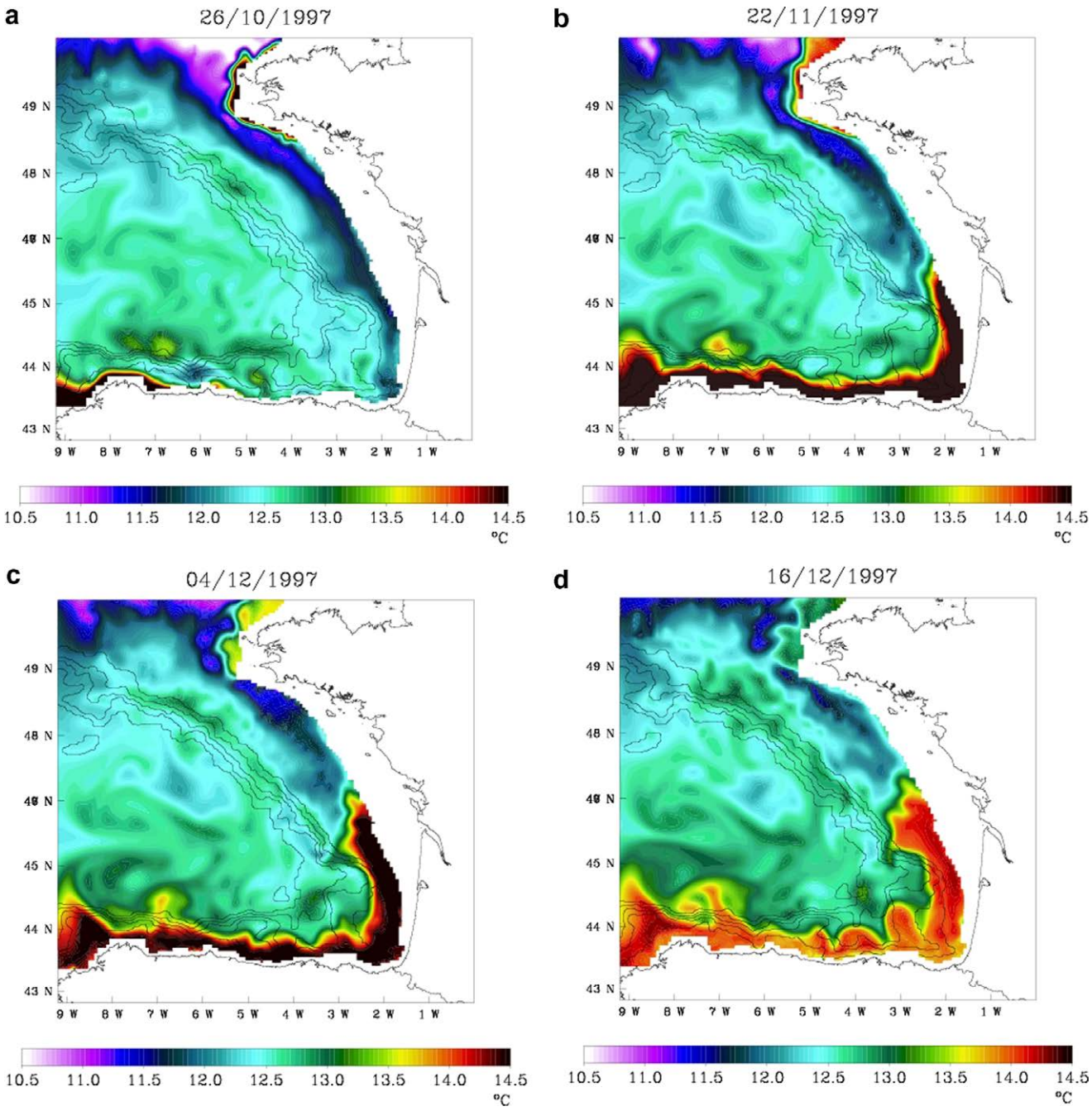


**Fig. 5.** Two-way nesting simulation. Four consecutive temperature snapshots at 75 m depth in late 1997 separated by a 15-day interval.

*4.2. Behaviour of the solution in the vicinity of the interface*

In this section, we focus on the impact of the different coupling methods on the solution near $\Gamma$, the western boundary of the regional domain. For such an evaluation, we have to impose some a priori requirements on the solution, and therefore to define some corresponding quantitative criteria. An optimal coupling method should make the interface perfectly transparent, i.e. should provide a solution which is as regular as possible through $\Gamma$. This typically means that the model variables and their fluxes should be continuous through $\Gamma$. Moreover no reflected waves nor energy or enstrophy accumulation should be observed along $\Gamma$. In order to diagnose a possible accumulation of energy at the boundary, we computed the zonal evolution of the total kinetic energy TKE, averaged in time over the three years of simulation and averaged meridionally:

$$\langle \overline{TKE} \rangle(x) = \frac{1}{2|S_x|T} \int_{S_x} \int_T [u^2 + v^2] \mathrm{d}t \, \mathrm{d}s \tag{5}$$

with $T = 3$ years, and where $S_x$ denotes a meridional section across the BABY15 domain, parallel to $\Gamma$. The corresponding curves are displayed in Fig. 6.

On the western side of the boundary, $\langle \overline{TKE} \rangle$ is weak because the resolution of the large model (1/3°) is not sufficient to allow the development of realistic mesoscale turbulence. In general, for each curve, the TKE strongly increases when going through $\Gamma$(9°W), due

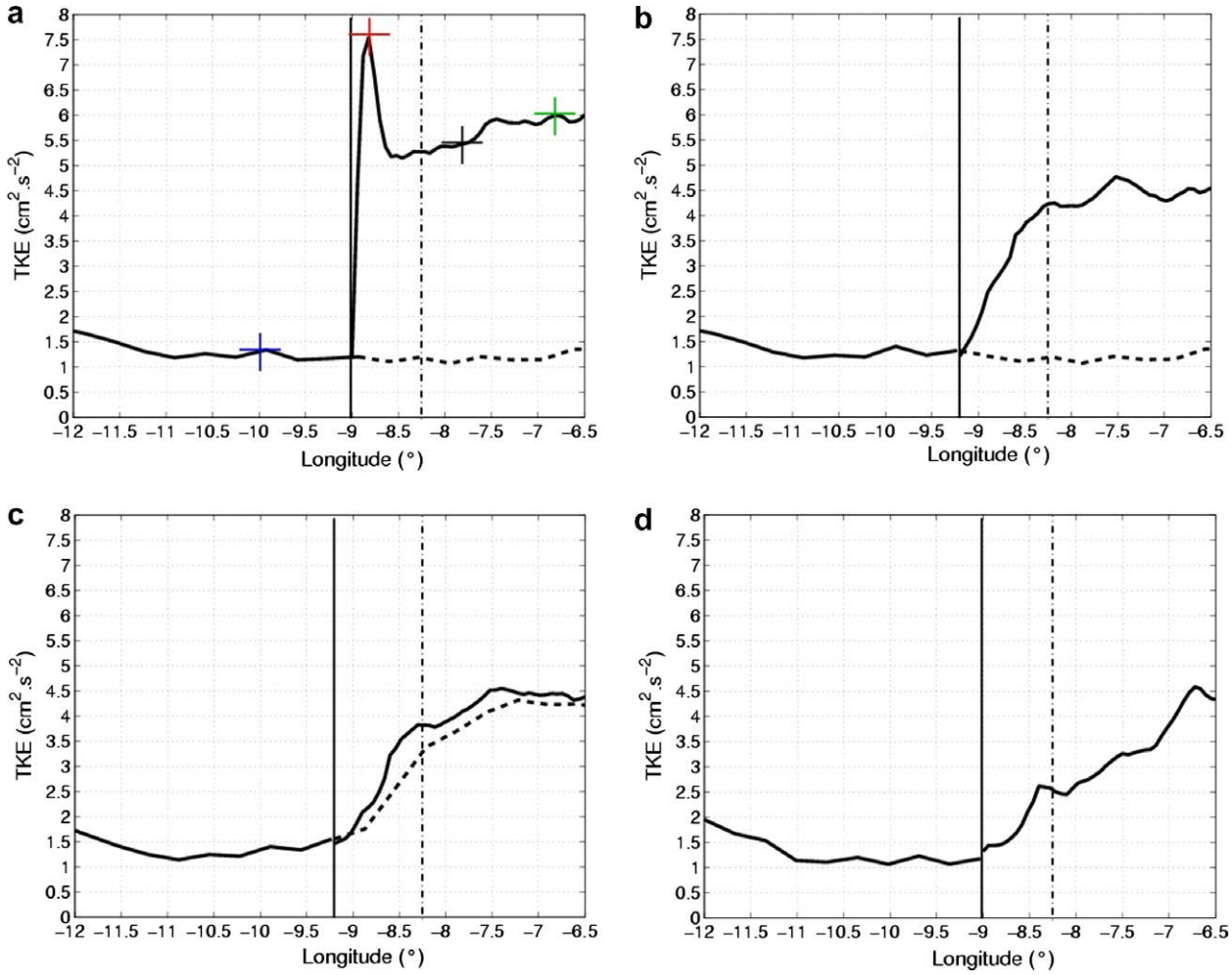


**Fig. 6.** Zonal variation in the time mean Total Kinetic Energy on each side of the western boundary of the BABY15 domain for the various simulations: (a) *BABY15-clamped*, (b) *1W-nesting*, (c) *2W-nesting*, and (d) *full-coupling*. The vertical solid line delimits the boundary of the BABY15 domain (at 9°W) or the interface between the two grids (at 9.2°W). The 1/3° is to the left and the 1/15° to the right. In (a) and (b), the solution in the coarse-resolution area is that of *NATL3-alone*. The vertical dashed line delimits the transition layer for bathymetry and viscosity/diffusivity. The dashed curve corresponds to the time mean TKE of the *NATL3-alone* simulation on the overlapping zone of the fine and coarse domains. The coloured crosses correspond to the sections used to calculate the time variation of the TKE in Fig. 7.

to the increase in resolution, and it reaches a threshold farther eastward inside the regional domain. This transition is the most progressive in the *full-coupling* experiment (Fig. 6d), and is slightly steeper in the *2W-nesting* (Fig. 6c). However no such smooth transition can be observed for the simulation with clamped BC (Fig. 6a), although the transition layer is also present in this model. Unlike the other simulations, the *BABY15-clamped* solution accumulates a lot of energy right at the boundary. Moreover, the TKE remains significantly higher inside the regional model, indicating that the energy trapped at the boundary propagates back into the BABY15 domain. Note that this accumulation of energy could have been reduced by the use of an additional "sponge layer" for a better damping of the flow along the boundary. This was not done for the purpose of a relevant comparison with the 1-W nesting, the main difference between these experiments then being the frequency at which boundary data are provided.

The increase of TKE from the boundary toward the interior of the fine-grid domain is much more progressive in the other simulations, even for the *1W-nesting* case (Fig. 6b), indicating a better performance of the coupling methods. Note that these three simulations (*1W-nesting*, *2W-nesting* and *full coupling*) lead to similar levels of TKE inside the fine-grid domain (eastern extremities of the curves), the transition being increasingly smooth with the sophistication of the method. In the *2W-nesting* and *full coupling* cases (Fig. 6c and d), the TKE in the coarse-resolution domain is different from that of the one-way or clamped cases, on account of the retroaction from the fine grid onto the coarser one.

To complete the above analysis, we consider the evolution of the TKE over time, spatially averaged along meridional sections near the western boundary in the large model (at 10°W) and in the regional model (at 8.8°W), and along sections further inside the regional domain at 7.8°W and 6.8°W.

$$\langle TKE \rangle(t) = \frac{1}{2|S_x|} \int_{S_x} [u^2 + v^2] \, \mathrm{d}s \tag{6}$$

This allows us to determine whether the accumulation of energy near the boundary evolves over time. The change in the TKE is shown in Fig. 7 for the *BABY15-clamped* and the *2W-nesting* simulations. For the *BABY15-clamped* simulation (Fig. 7a), the evolution of the TKE over time at the 10°W section (blue curve) is that of the *NATL3-alone* simulation. It remains weak without any strong fluctuations over time since the 1/3° resolution does not allow the generation of energetic mesoscale eddies. Near the boundary inside the regional model at 8.8°W (red curve), the TKE level is high, with strong (unrealistic) high frequency fluctuations persisting over the 3 years of simulation. This confirms the poor propagation of energy

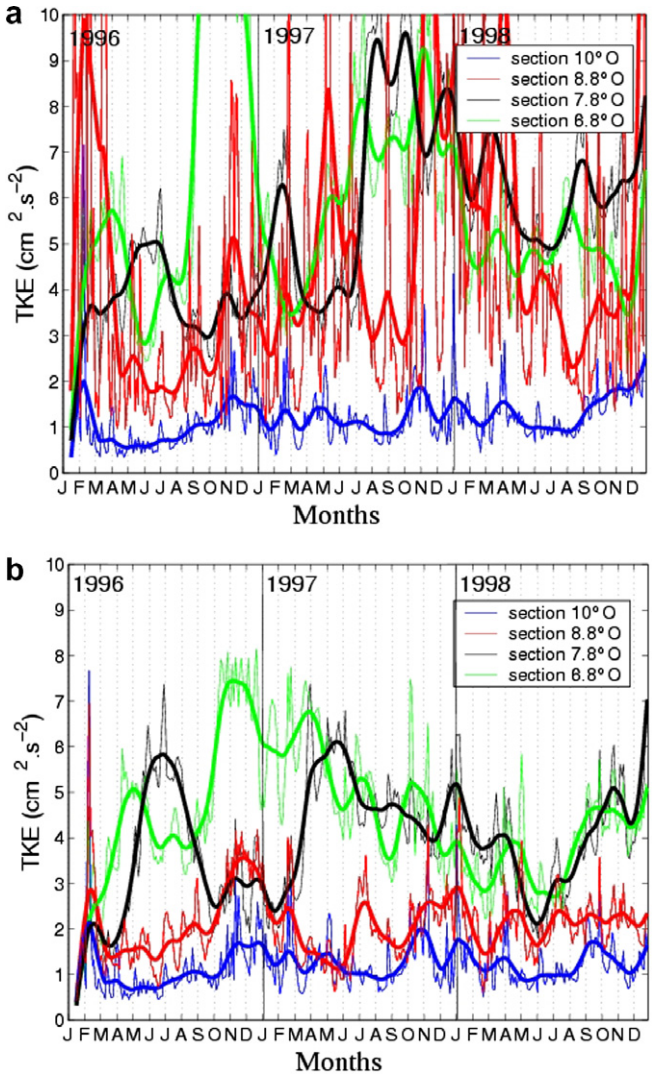


**Fig. 7.** Time variation during the 3-year integration of the Total Kinetic Energy at several meridonal sections parallel to the 9°W open boundary of the BABY15 domain. Simulations (a) *BABY15-clamped* and (b) *two-way-nesting* are shown. The TKE has been spatially averaged along the sections. Sections are located in the coarse-resolution domain at 10°W and in the fine-resolution domain at 8.8°W, 7.8°W and 6.8°W, as they are indicated in Fig. 6. The thin curves are instantaneous values, while the thick curves are smoothed with a 30-day running average.

through the boundary and is consistent with the accumulation described above. Further inside the regional domain, at 7.8°W and 6.8°W (black and green curves, respectively), the TKE level remains high but the high frequency fluctuations are much weaker (and more realistic) in amplitude. Moreover, it may be observed that the 30-day smoothed versions of these two curves curves exhibit similar behaviour over the last half of the simulation (mid-1997 to 1998): a marked seasonal cycle appears with a maximum of TKE in autumn and winter and a minimum in summer. During the season of maximum energy, whatever the section considered, we observe 2-month time-scale oscillations, which are probably associated with the strengthening of the slope current along the shelf break and the intensity of its pulses in response to the wind (Cailleau, 2004; Pingree and Le Cann, 1990). The time for the seasonal cycle to become established suggests a spin-up of about 18 months.

For the *2W-nesting* simulation (Fig. 7b), the evolution of the TKE as well as its levels on each side of the boundary (at 8.8°W and 10°W, red and blue curves, respectively), are very comparable, which demonstrates a certain continuity through the boundary. The amplitude of the high frequency variations is no larger in the transition layer than it is inside the regional domain, unlike that observed for the clamped boundary simulation. However, the spin-up phase of the regional domain also seems to last about 18 months, this being the time it takes for a clear seasonal cycle to appear in the 7.8°W and 6.6°W sections.

The behaviour of the TKE in the other two simulations (*1W-nesting* and *full coupling*, not shown here) is comparable to the *2W-nesting* case. TKE levels in the *1W-nesting* (respectively, *full-coupling*) simulation are globally slightly higher (resp. lower) than in the *2W-nesting* simulation. This is consistent with the analysis of the time mean TKE (Fig. 6): the Schwarz coupling and two-way nesting methods do not accumulate energy either near the boundary or further inside the regional domain.

To sum up this energy analysis, the transition of energy is most continuous and most progressive in the *2W-nesting* and *full-coupling* simulations. The clamped BC shows some difficulties in evacuating energy, unlike the other methods. Energy gets trapped along the boundary, but also radiates back into the interior. Note that the radiative boundary condition behaves in the same way. The one-way nesting – the principle of which is close to that of the clamped boundary, but with boundary data provided with time sampling equal to the coarse-grid time step (here 2400 s as opposed to 3 days for the clamped BC) – leads to a clear improvement of TKE behaviour near the boundary. Thus the time sampling of the boundary data appears to be an important element in controlling a model through its boundaries. This conclusion confirms the results of Blayo et al. (2006).

To complement the above energy analysis, we examined instantaneous maps of temperature (Fig. 8) and current velocity (Fig. 9) on August 13th 1998. This date was characterised by a situation of significant flows through the western boundary of the Bay of Biscay. The *BABY15-clamped* simulation shows by far the most marked discontinuities in the temperature field, as for example a cold anomaly near the boundary at about 48°N and a significant cold-water tongue along the Southern coast of Ireland (Fig. 8a). The associated current velocity field (Fig. 9a) shows a strong northward current along the 9° boundary which flows from 48°N to the southern tip of Ireland. Such a flow, which does not appear in the other simulations, is a clear artefact of the lack of permeability of the clamped boundary condition. Due to the continuity constraint, and again because the boundary condition does not let the flow through, this artificial northward flow turns eastward at the Irish coast, generating a strong coastal current in the direction of the Irish Sea. This latter coastal current flows in the opposite direction in all the other experiments (Figs. 9b–d). The nested simulations (Figs. 8b,c and 9b,c) and the *full coupling* simulation (Figs. 8d and 9d) enable better and more consistent flux behaviour at the boundary. The continuity of the temperature and flow patterns appears fairly well respected in two-way and coupled modes, which allows the coarse-grid solution to adjust at the western boundary. The transparency of the boundary is quite remarkable in the case of the full coupling simulation: the penetration of the North Atlantic Current in the Bay of Biscay at 47°N and the outflow of the upwelling current at 43°N are basically not disturbed.

In order to quantify these aspects of continuity through the boundary, we defined the following "continuity index":

$$I_\phi(t) = \left( \frac{1}{|\Gamma|} \int_\Gamma (\phi_{\text{large scale}}(y,t) - \phi_{\text{regional}}(y,t))^2 \mathrm{d}y \right)^{1/2} \quad (7)$$

which is a measure of the jump in the quantity $\phi$ through $\Gamma$ (and therefore has the same unit as the quantity). This index can be computed for different quantities, such as the horizontal velocity com-

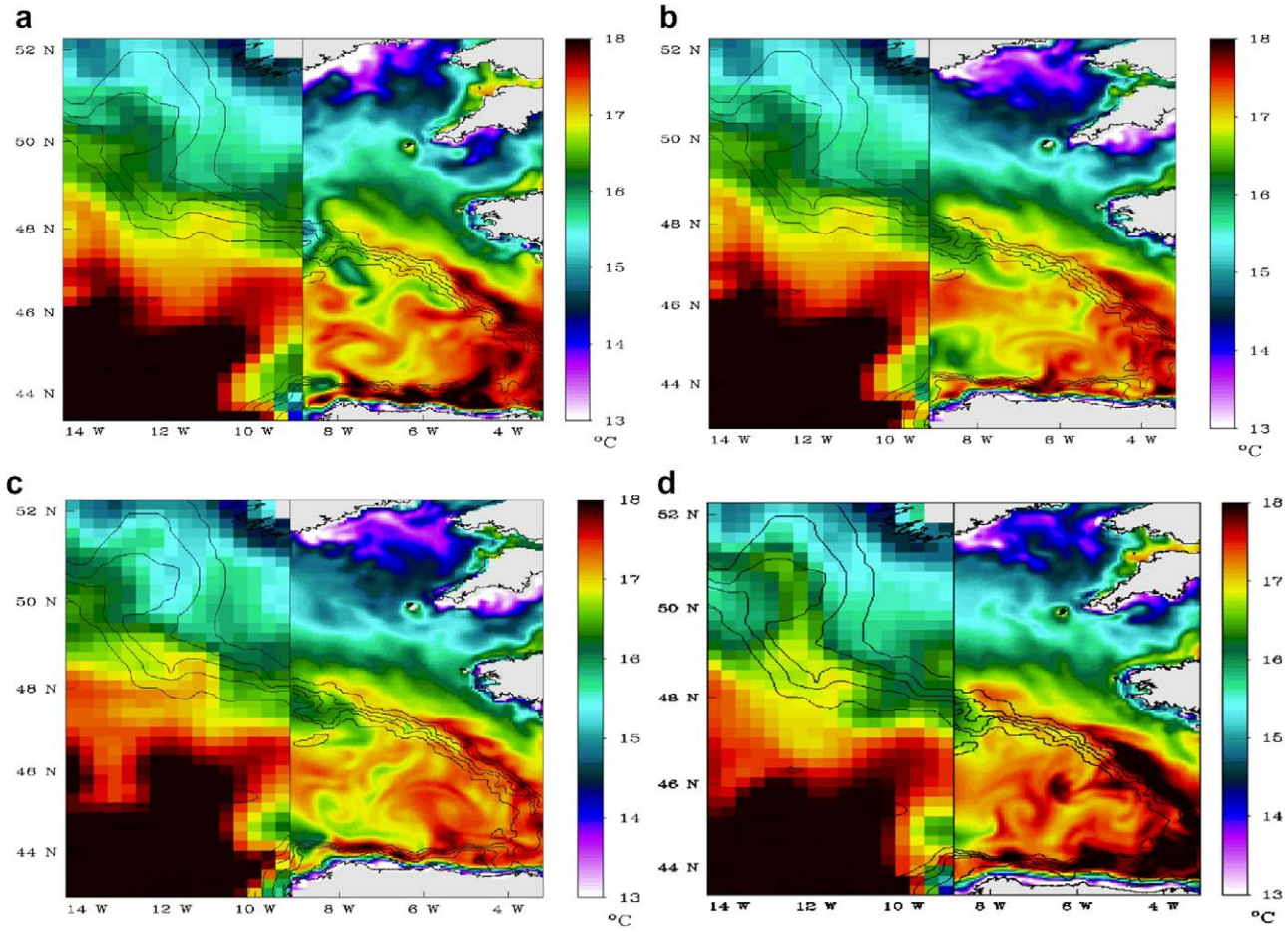


**Fig. 8.** Snapshot of the model temperature (colour) at 30 m depth on 13 August 1998, for the coarse-grid *NATL3* solution and the fine-gridit BABY15 solution on both sides of the western boundary of the regional domain and for the various simulations: (a) *BABY15-clamped*, (b) *one-way-nesting*, (c) *two-way-nesting*, and (d) *full-coupling*. The line at 9°W delimits the BABY15 domain. No interpolation is made in the plots, so coloured pixels have the size of the grid. Contour lines represent the bottom topography.

ponents $u$ and $v$, or their zonal gradients $\frac{\partial u}{\partial x}$ and $\frac{\partial v}{\partial x}$. A smaller value for the index indicates better continuity across the boundary.

Table 2 displays the mean continuity index of the velocity components at 30 m and of their derivatives normal to the boundary, for the different simulations. It confirms the previous analyses. The indexes of the clamped boundary simulation are the largest of all the simulations, especially for meridional velocity (i.e. tangential velocity). The continuity index of $v$ is three to five times smaller than those of the other boundary conditions. This strong discontinuity of the *BABY15-clamped* solution is consistent with the recirculation problem along the boundary, shown above in the velocity map (Fig. 9). The continuity indexes of other boundary conditions are similar, with nevertheless the best results being observed for the two-way methods, *2W-nesting* and *full-coupling*. This latter simulation allows the smallest continuity index on the derivatives of the velocity, hence an improved representation of the vorticity field near the boundary (figure not shown).

The evolution of the continuity index over time is shown in Fig. 10 for $u$ and $v$ at 30 m and for their normal derivatives. The same observations may be made as for the mean values. The *BABY15-clamped* method performs worst, especially on $v$, $u$ and $\partial v/\partial x$. Comparing the two-way methods, the 2W-nesting performs better on the fields, and the full coupling on their derivatives. The smallest discrepancies between methods are observed for the $u$-derivative, probably because of the constraint of volume flux conservation across the boundary. Finally, it is interesting to note that the value of the continuity index is set very quickly at the beginning of the experiment and remains steady (with seasonal variations) throughout the simulation. Thus discontinuity at the boundary does not decrease after spin-up, unlike the TKE.

### *4.3. Impact inside the regional domain*

We now focus on the impact of the different methods on the solution for the interior of the regional domain. Fig. 11 shows the variations in the TKE spatially averaged over the regional domain for the period 1996–98. These curves first show a spin-up phase due to the dynamical adjustment which seems to depend on the method used for the processing of boundary conditions. In the case of the clamped boundary (Fig. 11a), the increase in TKE is very marked over the first two months, and the TKE level remains high throughout the first year. This method leads to a higher energy level in the regional model than the others methods. For the *1W-nesting* and *2W-nesting* simulations, the assessment is more satisfactory, i.e. the initial increase is clearly weaker but continues to develop over the first year. We can observe a lower threshold in the two-way mode. For the coupled simulation, the increase is relatively marked during the first two months, but, unlike all the other simulations, the increase in the TKE does not continue after the initial phase. It even shows a decreasing trend during the last phase of the experiment. We have not examined the reasons for such behaviour yet.

It is interesting to note that every simulation shows a similar well marked seasonal cycle (higher TKE from October to April). This cycle, already seen on the TKE at the boundary, does not seem

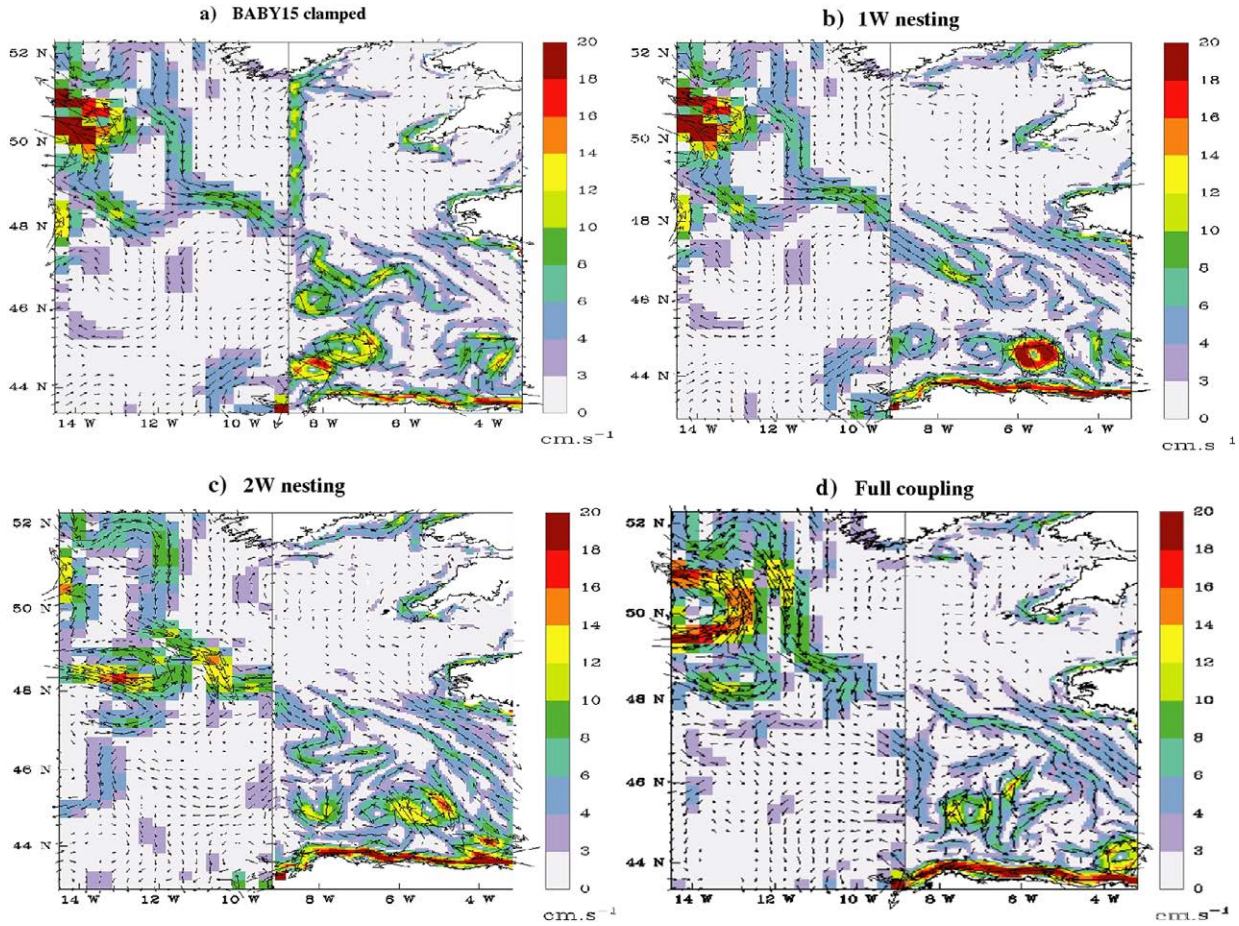


**Fig. 9.** Same as Fig. 8, but for the velocity field at 30 m. The direction of the current is shown by arrows, and the speed of the currents by the colour scale (in cm/s).

to be influenced by the boundary conditions used in this study, suggesting that the seasonal cycle of the circulation in the regional model is not very dependent on the boundary condition used.

The time evolution from mid 1997 to the end of 1998 of an observation based estimate of the surface TKE is shown in Fig. 12. This TKE is referred to as the observed TKE hereafter. It is calculated from the surface absolute geostrophic current estimates provided by the SSALTO/DUACS analysis of satellite altimetry (http://www.aviso.oceanobs.com/duacs/). The surface TKE obtained from the various model simulations are also reported in Fig. 12. Although model TKE and observed TKEs do not represent exactly the same quantity (the later does not include ageostrophic contributions such as the Ekman currents), their comparison is useful in our attempt to rank the various methods. We chose this 18-month period because it corresponds to a period when the dynamical spin-up of the regional model is basically achieved. The mean level of the observed TKE is about 70 $cm^2/s^2$. It shows a well marked seasonal cycle, the amplitude of which is about 10 $cm^2/s^2$, the maximum TKE values occurring during winter time between October and April. Variations of smaller amplitude at monthly time scale are seen, sign of a noticeable mesoscale eddy activity. These features are qualitatively well reproduced in all model experiments, except for the mean TKE level which is significantly smaller (30–35 $cm^2/s^2$ smaller), despite it includes an ageostrophic contribution. The amplitudes of the seasonal cycle and of the monthly time scale modulation of the models TKE compare well with observations, even when we extend the comparison over the whole 1996–1998 period. Significant (to the 99% level) correlation coefficients, calculated over the full 3 year period to increase the significance, between model and observed TKE time series are, respectively, 0.70 for *clamped*, 0.75 for *1W-nesting*, 0.76 for *2W-nesting*, and 0.79 for *full-coupling*. Biases and rms (not shown) also improve in the same order, which confirms the "ranking" of the methods in that order, as already suggested by the analysis of the OBCs at the vicinity of the boundary (Table 2). The small differences between the various experiments also confirm the previous comments that differences in OBCs are not crucial for the simulation of the seasonal variability of the kinetic energy in the domain, which is dominated by the wind forcing. However, the clamped boundary condition has an impact of the mean TKE level,

**Table 2**
Mean continuity index through the boundary $\Gamma$ for the $u$ and $v$ components of velocity, and for their normal derivatives

| Simulations | BABY15 clamped | 1W nesting | 2W nesting | Full coupling |
|---|---|---|---|---|
| $I_u(t)$ (m $s^{-1}$) | 0.048 | 0.036 | 0.025 | 0.028 |
| $I_v(t)$ (m $s^{-1}$) | 0.082 | 0.033 | 0.015 | 0.026 |
| $I_{\partial u/\partial x}(t)$ ($10^{-6}$ $s^{-1}$) | 2.110 | 1.904 | 2.012 | 1.578 |
| $I_{\partial v/\partial x}(t)$ ($10^{-6}$ $s^{-1}$) | 6.639 | 3.246 | 2.879 | 2.609 |

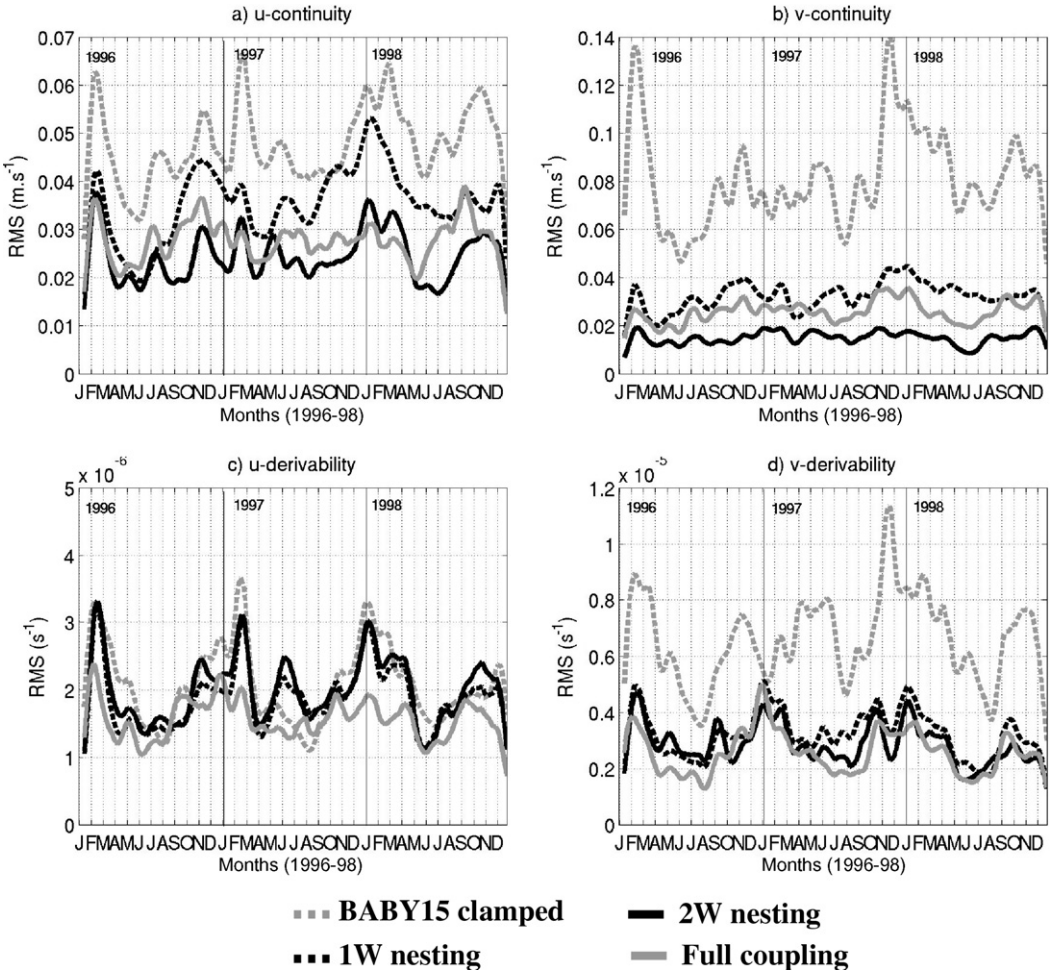


**Fig. 10.** Variations in the *continuity index* over time for the velocity components and their derivatives normal to the boundary for every experiment (see text for the definition of that index).

and we cannot exclude that the other boundary schemes do not contribute also to the underestimation of the TKE in the models.

To better understand the reason for this similarity in the seasonal cycle, we looked at the circulation along the shelf break in the Bay of Biscay. We examined the changes in volume transport through two sections normal to the shelf break, during the third year (Fig. 13), after sufficient time had elapsed following spin-up. These sections are indicated in Fig. 2. The first section (Galicia) is a meridional section at 7°W, and not far from the southern entrance to the domain (at 9°W). The second section (Armorique) is oblique, centred on 45°N, and at some distance from the open boundary. Regarding the Galicia section (Fig. 13a), the correlation between the transport curves of the different simulations is not obvious. Nevertheless, we notice a maximum eastward transport in autumn for every simulation, and a reversal of the current to the west in winter (December and January). This section is close to the boundary and its transport is logically sensitive to the BCs. In addition, this region is subject to strong and chaotic mesoscale activity: topographic canyons make the current unstable along the shelf break and energetic eddies are generated. The evolution of these eddies could be strongly influenced by the boundary conditions, especially since they tend to drift westward. This internally generated eddy field also contributes to the low correlation observed between the different transport time series through the Galicia section, given that one particular eddy could very well create a temporary reversal of the current in a given simulation. Nevertheless, the clamped boundary simulation (*BABY15-clamped*) is again the one that exhibits the most different behaviour. In fact, for this section dominated by strong mesoscale activity, ensemble simulations or longer periods of simulation which could smooth out the perturbation due to locally generated turbulence, would be more appropriate to make the comparison of the mean transports through the Galicia section more informative. For the moment, we cannot conclude whether the observed differences are due to the decorrelation of mesoscale activity or to the boundary condition.

With regard to the Armorique section (Fig. 13b), the correlation between the transport time series is much clearer. Most curves show in-phase bi-monthly oscillations. The transport is generally southward from the end of winter and spring, and a northward flow begins in August, becoming strong in the autumn. The greatest transport occurs in November (except for the *1W-nesting* simulation). The maximum transport in autumn is in good agreement with the measured currents along the shelf break (Pingree and Le Cann, 1990). The current reverses again southward in December. This section is a long way from the boundary. Here variability in transport, which is primarily wind-driven, seems to depend little on the method used at the 9°W boundary, at least for the phase of the seasonal variations. The main differences between the simulations lie in transport intensity: in autumn the maximum transport is more distinct for the *2W-nesting* and *full-coupling* simulations, which have so far shown the best results. Again, due

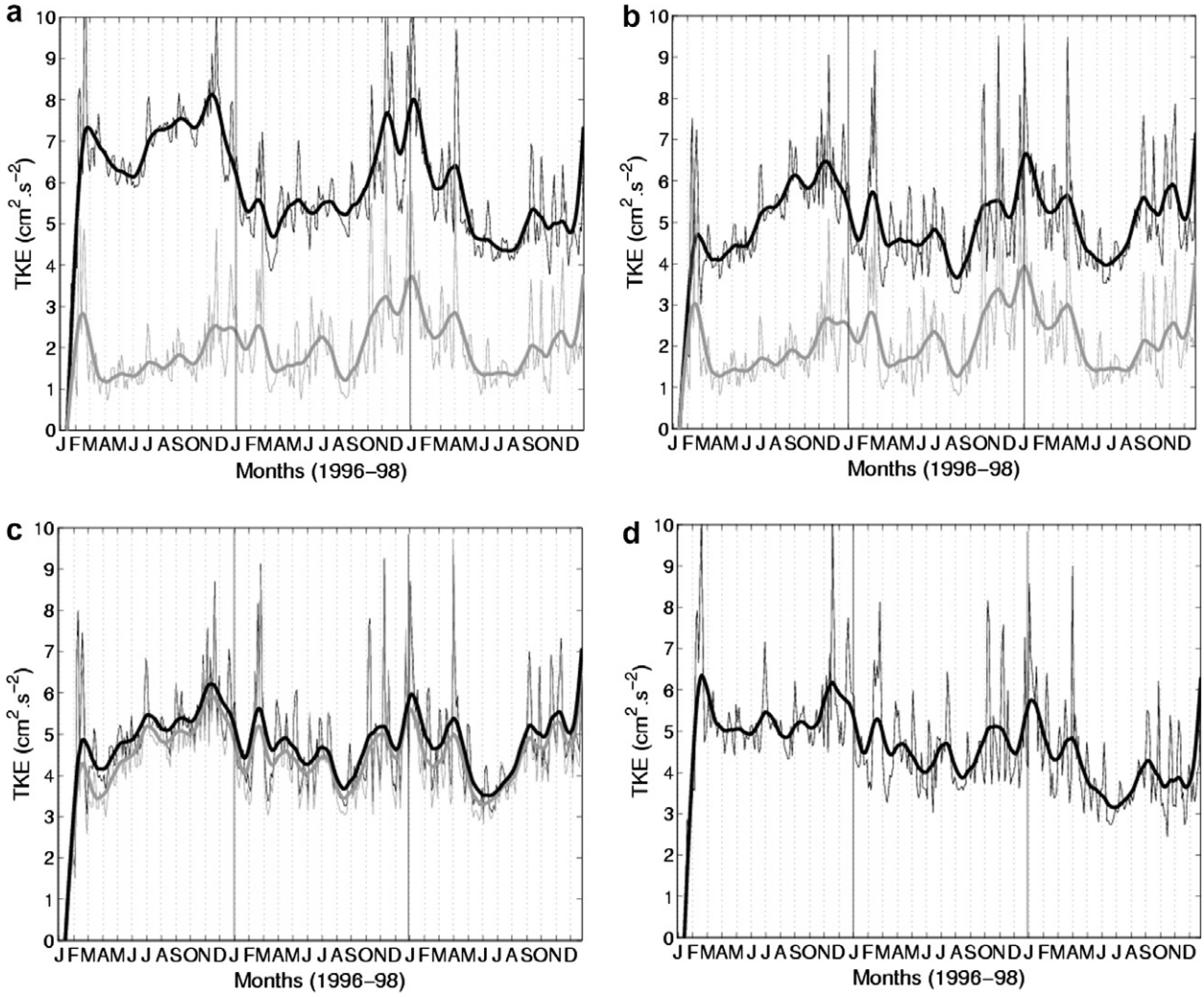


**Fig. 11.** Time evolution for the three-year integration of the TKE averaged on the whole regional domain for the various simulations: (a) *BABY15-clamped*, (b) *1W-nesting*, (c) *2W-nesting*, and (d) *full-coupling*. The black curve corresponds to the fine-grid solution, and the grey curve corresponds to the coarse-grid solution (i.e. the *NATL3-alone* solution for (a) and (b)). The thin curves are sampled every 3 days, and the thick curves are smoothed with a 30-day running average.

to mesoscale activity, we could not discriminate between the impact of the boundary conditions and that of mesoscale turbulence.

In an attempt to further evaluate the performance of the *full-coupling* method and the *2W-nesting* method, we compared their solutions to hydrographic observations over the 3 year period of 1996 to 1998. The fine grid model 3-day outputs were collocated in space and time with all hydrogaphic (*T*,*S*) observations available between the surface and 2000 m depth in the ENACT/ENSEMBLE data base between 1996 and 1998. A total of 1852 vertical *T*,*S* profiles were used, which correspond to nearly 42,000 individual *T* and *S* observations. Both the *full-coupling* and the *2W-nesting* solutions produced the same bias regarding the collocated observations (no figure shown), and it was not possible to assess which simulation approaches best the observations. Therefore, the two methods appear very equivalent in their ability to reproduce the local circulation.

## 5. Conclusion

In this study, we evaluated four different methods to constrain the open boundaries of a high-resolution (1/15°) regional ocean model of the Bay of Biscay using outputs from a coarser-resolution (1/3°) North Atlantic model. The clamped boundary condition and radiation condition are among the most commonly used open boundary conditions today, but systematically lead to energy accumulation and problematic recirculations along the boundary. The continuity of the variables and their derivatives at the boundary is poorly handled. This type of boundary condition can disturb the internal dynamics of the regional domain. Moreover, model solutions provided by these methods are largely dependent on the frequency with which the values of the variables imposed at the boundaries are updated. The reflectiveness of the clamped boundary condition has much weaker consequences in the one-way nesting solution, for which boundary values are updated at every time step of the coarse-resolution model (basically every hour). However, we have to point out that similar OBCs, based on the method of characteristics, are much more appropriate and perform better in the context of ocean models (Blayo and Debreu, 2005a). Such methods are still not fully operating for the baroclinic part of the primitive equations, but can already easily be used at least for the barotropic part.

The one-way or two-way-nesting and full-coupling methods tested here behave in a far more satisfactory manner. The boundary is more transparent, continuity of model variables across the boundary is better, and the circulation inside the regional domain does not seem to be significantly disturbed by artificial motion

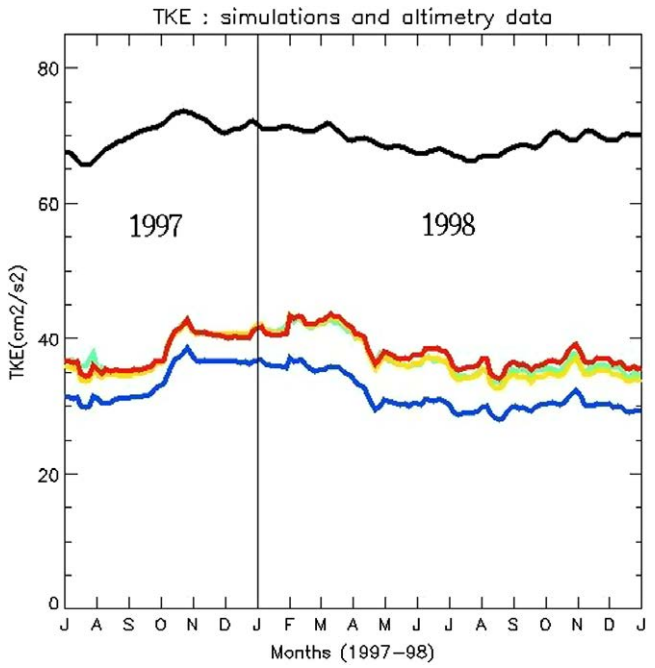


**Fig. 12.** Comparison of the time evolution for the 18-month period (July 1997–December 1998) of the surface TKE averaged on the whole regional domain. Top–down: data obtained from Topex/Poseidon satellite altimetry data from SSALTO/DUACS (black), full coupling (green), two-way (red), one-way (yellow), clamped (blue). (For interpretation of the references to color in this figure legend, the reader is referred to the web version of this article.)

generated at the boundary. For long periods of integration, the two-way mode improves both the fine- and coarse-grid solutions. In return, the large-scale model has to be integrated simultaneously with the regional model. This is quite feasible if the cost of the large model is no more than a part of the cost of the regional model (in our case 50%). Finally, the full-coupling method (the Schwarz method) was found to provide the most regular solution at the boundary, assuring good continuity of the model variables, and the best continuity (among all the methods) of model variable derivatives (especially vorticity). With this method, the boundary is remarkably transparent. However, the method requires much more computation time because it uses an iterative algorithm (both models need to be integrated several times, typically 5 for the results presented here), and requires optimisation. Nevertheless, the method opens up some interesting perspectives because it should enable to couple models with different physics. This is particularly interesting when the finest resolution model solves another dynamics (e.g. non-hydrostatic).

Regarding which scheme to recommend, the answer is not straightforward since it depends on application. For example, if one has high frequency sampled boundary data available, and if one is not concerned by the details of the flow close to the boundary, the radiation condition (or clamped condition) with a proper transition layer will do a fairly good job at a low cost, despite the fact that this method is mathematically erroneous. If one has not very high quality boundary data available, better OBCs should be used (Blayo and Debreu, 2005a).

If two-way interaction is computationally affordable, our results demonstrate that the full-coupling method is the most satisfactory because of the mathematical regularity of the solution (continuity and differentiability) at the boundary. However, our result could not demonstrate that this improvement of regularity, which is achieved at a very high computational cost (an increase by a factor of 5), significantly improves the simulation of the ocean physics in the BABY15 domain compared to the two-way nesting method. Both methods appear to produce very similar solutions in the interior of the fine grid model. Such a demonstration could not be achieved in the present set-up. It is likely that the improvement we are looking for is quite small, errors in the 2W-nesting and Full-Coupling solutions being likely dominated by model/forcing errors rather than errors induced by the differences in the nesting algorithms. Quantification of such differences would require, on one hand, a larger number of longer experiments, but also a proper observation data base that would allow a correct initialisation of the model and an accurate and quantitative assessment of the simulations. In the Bay of Biscay, the lack of long term currents records of the slope current, a critical element to validate the flow through the boundary, is a considerable handicap. Another region of the ocean, more densely observed, will have to be chosen. On the other hand, it might be necessary in the future to use more classical comparison approach, less sensitive to model/forcing

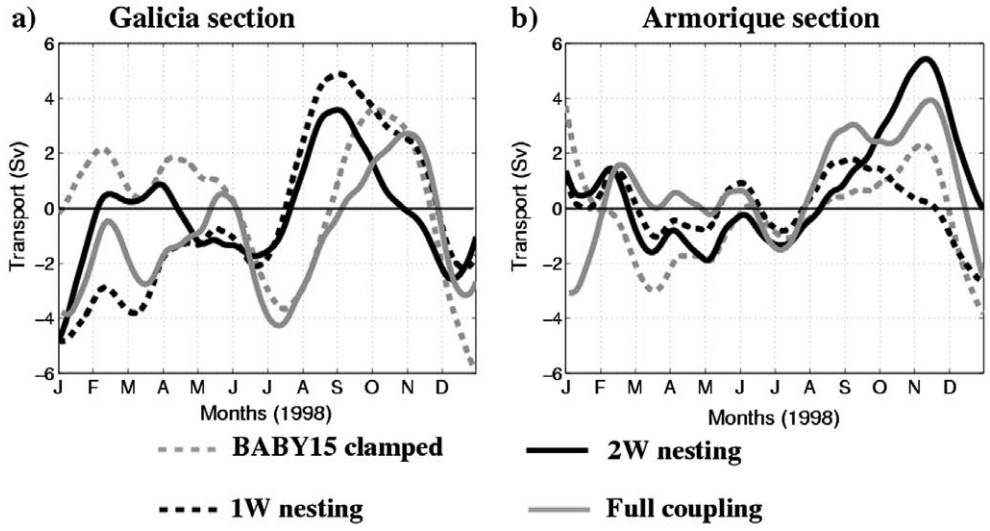


**Fig. 13.** Evolution of the current transport along the shelf break of the Bay of Biscay in 1998 for the various simulations. (a) Transport through the Galicia meridional section at 7°W, (b) Transport through the Armorique oblique section. These two sections are indicated in Fig. 2. Positive (negative) values mainly indicate eastward (northward) transport across the Galicia (Armorique) section.

errors, in which a high-resolution parent domain simulation is used to evaluate the performances of the nesting methods. At present, we recommend to use the two-way method. However, it is a rather demanding approach, since the set up of the large scale model and forcing has to be carefully mastered.

Finally, we evoked the problem of the spin-up phase. In this study, initial conditions for temperature and salinity were obtained from a higher resolution experiment, and the model was started from rest. Whichever boundary condition was used, the regional model needed about 18 months to reach a dynamical equilibrium. Thus, for short periods of integration as in operational ocean forecasting, it will be necessary to improve the methods of initialisation. Variational methods like those proposed by Auclair et al. (2000) are promising in this respect.

## Acknowledgements

Supports from DGA, CNRS and UJF are acknowledged by the authors. This study was supported by grants from SHOM, CNRS/INSU, CNES and the French national program GMMC to both the COMODO and to the CLIPPER projects. We acknowledge the support of Institut du Développement et des Ressources en Informatique Scientifique (IDRIS) in Orsay, where numerical calculations were performed. The authors are also grateful to Dr. Thierry Penduff and Mélanie Juza for the comparison of simulation results with hydrographic observations, and to Dr. Laurence Viry for her help in managing the data.

## References

Auclair, F., Casitas, S., Marsaleix, P., 2000. Application of an inverse method to coastal modelling. J. Atmos. Ocean. Technol. 17, 1368–1391.

Barnier, B., 1998. Forcing the Ocean. In: Chassignet, E.P., Verron, J. (Eds.), Ocean Modeling and Parameterization. Kluwer Academic Publishers, The Netherlands, pp. 45–80.

Barnier, B., Marchesiello, P., De Miranda, A., Molines, J., Coulibaly, M., 1998. A sigma-coordinate primitive equation model for studying the circulation in the South Atlantic. Part I: Model configuration with error estimates. Deep Sea Res. 45, 543–572.

Blayo, E., Debreu, L., 2005a. Revisiting open boundary conditions from the point of view of characteristic variables. Ocean Modell. 9, 231–252.

Blayo, E., Debreu, L., Dumas, F., Garnier, V., Marin, J., Robert, C., Vandermeirsch, F., 2006. Investigation of 2-D and 3-D characteristic open boundary conditions for regional ocean models. In: Proceedings of the Coastal Operational Oceanography conference, Brest, october 2006.

Cailleau, S., 2004. Validation de méthodes de contrainte aux frontières d'un modèle océanique: application à un modèle hauturier de l'Atlantique Nord et à un modèle régional du Golfe de Gascogne. Ph.D. Thesis, Université Grenoble 1.

Chanut, J., Barnier, B., Large, W., Debreu, L., Penduff, T., Molines, J.M., 2008. Mesoscale eddies in the Labrador Sea and their contribution to convection and restratification. J. Phys. Oceanogr, in press.

Debreu, L., 2000. Raffinement adaptatif de maillage et méthodes de zoom, application aux modèles d'océan. Ph.D. Thesis, Université Joseph Fourier, Grenoble, France.

Debreu, L., Blayo, E., Barnier, B., 2004. A general adaptive multiresolution approach to ocean modelling. Experiments in a primitive equation model of the North Atlantic. In: Adaptive mesh refinement – theory and applications. In: Plewa, T., Linde, T., Weirs, V.G. (Eds.), Lecture Notes in Computational Science and Engineering, vol. 41.

Debreu, L., Vouland, C., Blayo, E., 2008. AGRIF: adaptive grid refinement in Fortran. Comput. Geosci. 34, 8–13.

Fox, A., Maskell, S., 1995. Two-way interactive nesting of primitive equation ocean models with topography. J. Phys. Oceanogr. 23, 2977–2996.

Givoli, D., 1991. Non-reflecting boundary conditions. J. Comput. Phys. 94, 1–29.

Holstad, A., Lie, I., 1999. On transparent boundary conditions and nesting for ocean models. Research Report 91, Norwegian Meteorological Institute, Oslo, Norway.

Hall, N., Barnier, B., Penduff, T., Molines, J.-M., 2004. Interannual variation of Gulf Stream heat fluxes in a high resolution model forced by reanalysis data. Clim. Dynam. 23, 341–351.

Huthnance, J., 1984. Slope current and 'jebar'. J. Phys. Oceanogr. 14, 795–810.

Lumpkin, R., Speer, K.G., Koltermann, K.P., 2008. Transport across 48°N in the North Atlantic Ocean. J. Phys. Oceanogr. 38, 733.

Madec, G., Delecluse, P., Imbard, M., Levy, C., 1998. OPA, release 8, ocean general circulation model reference manual. Internal Report, LODYC/IPSL, Paris.

Marchesiello, P., McWilliams, J., Shchepetkin, A., 2001. Open boundary conditions for long-term integration of regional oceanic models. Ocean Modell. 3, 1–20.

Martin, V., 2003. Méthodes de décomposition de domaine de type relaxation d'ondes pour des équations de l'océanographie. Ph.D. Thesis, Université Paris 13.

Martin, V., 2005. An optimized Schwarz waveform relaxation method for unsteady convection diffusion equation. Comput. Fluids 33, 829–837.

Orlanski, I., 1976. A simple boundary condition for unbounded hyperbolic flows. J. Comput. Phys. 21, 251–269.

Palma, E.D., Matano, R.P., 1998. On the implementation of passive open boundary conditions for a general circulation model: the barotropic mode. J. Geophys. Res. 103 (C1), 1319–1341.

Penduff, T., Barnier, B., Dewar, W.K., O'Brien, J.J., 2004. Dynamical response of the oceanic eddy field to the North Atlantic Oscillation: a model-data comparison. J. Phys. Oceanogr. 34, 2615–2629.

Penduff, T., Barnier, B., Molines, J.-M., Madec, G., 2005. On the use of current meter data to assess the realism of ocean model simulations. Ocean Modell. 11, 399–416.

Penven, P., Debreu, L., Marchesiello, P., Williams, J., 2003. Applications of the ROMS embedding procedure for the Central California Upwelling System. Ocean Modell.

Penven, P., Debreu, L., Marchesiello, P., McWilliams, J.C., 2006. Evaluation and application of the ROMS 1-wway embedding procedure to the central California upwelling system. Ocean Modell. 12, 157–187.

Perkins, A.L., Smedstad, L.F., Blake, D.W., Heburn, G.W., Wallcraft, A.J., 1997. A new nested boundary condition for a primitive equation ocean model. J. Geophys. Res. 102, 3483–3500.

Pingree, R., Le Cann, B., 1990. Structure, strength and seasonality of the slope currents in the Bay of Biscay region. J. Mar. Bio. Ass. UK 70, 857–885.

Pingree, R., Le Cann, B., 1992. Three anticyclonic slope water eddies (swoddies) in the southern Bay of Biscay in 1990. Deep Sea Res. 39, 1147–1175.

Reynaud, T., Legrand, P., Mercier, H., Barnier, B., 1998. A new analysis of hydrographic data in the Atlantic and its application to an inverse modelling study. Int. WOCE Newslett. 32, 29–31.

Smith, W., Sandwell, D., 1997. Global seafloor topography from satellite altimetry and ship depth soundings. Science 277, 1956–1962.

Treguier, A.-M., Reynaud, T., Pichevin, T., Barnier, B., Molines, J.-M., de Miranda, A.P., Messager, C., Beismann, J.O., Madec, G., Grima, N., Imbard, M., Le Provost, C., 1999. The CLIPPER project: high resolution modelling of the Atlantic. Int. WOCE Newslett. 36, 3–5.

Tréguier, A.-M., Barnier, B., de Miranda, A.P., Molines, J.-M., Grima, N., Imbard, M., Madec, G., Messager, C., 2001. An eddy permitting model of the Atlantic circulation: evaluating open boundary conditions. J. Geophys. Res 106 (C10), 22115–22130.

Treguier, A.-M., Gourcuff, C., Lherminier, P., Mercier, H., Barnier, B., Madec, G., Molines, J.-M., Penduff, T., Czeschel, L., Böning, C., 2006. Internal and forced variability along a section between Greenland and Portugal in the Clipper Atlantic Model. Ocean Dyn. 56, 568–580.

Tsynkhov, S.V., 1998. Numerical solutions of problems on unbounded domains. A review. Appl. Numer. Math. 27, 456–532.

Willebrand, J., Barnier, B., Böning, C., Dieterich, C., Killworth, P., LeProvost, C., Jia, Y., Molines, J.M., New, A.L., 2001. Circulation characteristics in three eddy-permitting models of the North Atlantic. Prog. Oceanogr. 48, 123–162.